Coronary centerline tracking in CT images with use of image moments and of an elastic model

Release 0.02

Marcela Hernández Hoyos[1], María Alejandra Zuluaga Valencia[1,2], Mónica Lozano[1], Juan Carlos Prieto Bernal[1], Philippe C. Douek[2], Isabelle E. Magnin[2],and Maciej Orkisz[2]

July 2, 2008

[1]Grupo Imagine, Grupo de Ingeniería Biomédica, Universidad de los Andes, Bogota, Colombia
http://agamenon.uniandes.edu.co
[2]Université de Lyon; Université Lyon 1; INSA-Lyon; CNRS UMR 5220, CREATIS; Inserm U630; F-69621 Villeurbanne, France
http://www.creatis.insa-lyon.fr

Abstract

This coronary-artery extraction method uses one initialization point per vessel. First, a mask is computed by use of a region-growing algorithm, which starts from the initial point and stops when no more connected voxels fall within a predefined intensity range. The centerline tracking is then performed within the mask, starting from the same initial point. This algorithm is based on a prediction/estimation scheme. It uses the first- and second-order image moments calculated within a spherical volume that slides along the vessel, and the radius of which is automatically adjusted to the local radius of the vessel. The evolution of the radius of the sphere is based on the analysis of the eigenvalues of the inertia matrix in a multi-scale framework. The estimation of the current point location makes use of an elastic model similar to ”snakes”. The point iteratively moves under the action of an image-force attracting it to the local gravity center, and under the reaction of the internal forces of the model, which reflect its shape constraints: continuity and smoothness. The prediction makes use of the eigenvectors of the inertia matrix. The stopping criteria of the centerline tracking are based on the size of the sphere and on the percentage of the masked voxels within the sphere.

On 8 training CT datasets, the following mean results were obtained. Overlap with reference: considering the whole length (OV) 80.1%, until the first failure (OF) 48.9%, in clinically relevant segments (radius $>$ 1.5 mm, OT) 81.7%. Average distance from reference: considering the whole length (AD) 4.32 mm, limited to segments where the semiautomatic centerline remains within the vessel (AI) 0.39%, in clinically relevant segments (AT) 4.13%. On 16 testing datasets, these results were respectively: OV $=$ 80.2%, OF $=$ 39.3%, OT $=$ 82.1%, AD $=$ 5.05 mm, AI $=$ 0.41 mm and AT $=$ 4.58 mm. A number of failures was due to the the fact that the model does not handle the bifurcations.

Latest version available at the Insight Journal [http://hdl.handle.net/1926/1338]

Contents

This paper describes a method submitted to the first Coronary Artery Tracking contest (CAT08: http://cat08.bigr.nl/) held in conjunction with the MICCAI 2008 conference http://miccai2008.rutgers.edu/.

1 State-of-the-art

Coronary artery disease remains one of the leading causes of death each year. Therefore, the evaluation of these vessels is of critical importance. Although manual delineation is still used in clinical routine, the amount of data that is processed nowadays makes automatic and semiautomatic segmentation a challenge.

Methods for centerline extraction can be broadly classified into two groups. On one hand, some methods perform an initial segmentation of the vessel followed by the centerline extraction [1]. Among these, the preferred centerline extraction technique is the skeletonization of the segmented structure. On the other hand, there are methods that perform a tracking of the centerline prior to the segmentation [3, 9] or simultaneously [8, 5, 6, 2, 4]. Main techniques used under this category include multi-scale Hessian analysis, inertia moments analysis, Bayesian approaches and minimal paths.

Some of these methods have not been originally developed to work over coronary arteries in CT images, but most of them have already been tested in this context. The main challenges still remain the correct managing of bifurcations, of severe stenoses and of adjacent hyper-intense structures.

2 Method

The core of the method is a minimally interactive centerline-tracking algorithm (section 2.2). According to the definition given by the organizers of CAT08, an algorithm is minimally interactive if the interaction is limited to manual definition of one point per vessel. Our algorithm was initially developed to be used in contrast-enhanced magnetic resonance images, and is based on the assumption that the vessels are high-intensity thread-like objects on low-intensity background. As this assumption is not met in CT images representing the coronary arteries, a preprocessing step was added (section 2.1), which intends to remove as many surrounding structures as possible.

2.1 Image preprocessing

The preprocessing step is actually a very coarse presegmentation that provides a connected set $\mathcal{V}_{pre}$ of voxels, the intensities of which fall within a range of values likely to correspond to arteries. A region-growing process is carried out starting from a user-defined seed point. Neighboring voxels are iteratively added to $\mathcal{V}_{pre}$ as long as they fall within a preset range $[T_L, T_H]$. We used the range proposed in [1], i.e. an upper bound $T_H = 876$ HU and a lower bound $T_L = 181$ HU. However, in the LCX arteries we preferred a different preset value of the lower bound: $T_L = 166$ HU. Let us note that this range includes both the arterial lumen and calcifications.

2.2 Centerline-tracking algorithm

Hereafter, we give an overview of the algorithm. More details can be found in our previous publications [6, 7]. The algorithm extracts the centerline of one vessel of interest, starting from a point within its lumen, the same one that was previously used to initialize the preprocessing. It includes the following steps:

- refinement (estimation) of the current point location $\mathbf{x}_i$;
- estimation of the local orientation of the vessel $\mathbf{e}_i$;
- prediction of the next (candidate) point $\hat{\mathbf{x}}_i$ according to this orientation.

Each of them uses first- or second-order image moments computed within a spherical sub-volume called *analysis cell*. We use a multi-scale framework to determine the locally most suitable size of the cell. The iterative tracking process is carried out in two opposite directions from the starting point, and stops when one of the stopping criteria is encountered. In CT images of the coronary arteries, the tracking process is carried out within the subvolume masked by $\mathcal{V}_{pre}$, and the stopping criteria (see section 2.2) are related to the presegmentation step.

Estimation of the current point location

Each centerline point is expected to coincide with the gravity center of the analysis cell. However, to cope with various undesired effects (noise, pathologies, nearby structures etc., we enforce continuity and smoothness of the centerline by means of a model similar to the well-known ”snakes”. The location of the current (predicted) point is iteratively refined under the action of an image-based *external* force and the reaction of the *internal* forces of the model. The *external* force attracts the point toward the center of gravity $\mathbf{x}_i^G$ of the cell centered in $\hat{\mathbf{x}}_i$. The *internal* forces reflect shape constraints of the model, namely continuity weighted by a coefficient w_c and smoothness weighted by w_s. The best empiric values of these parameters, $w_c = 0.5$ and $w_s = 0.1$, were determined from numerous tests.

The displacements due to internal and external forces are iteratively recalculated as long as the resulting displacement is larger than a fixed minimum value. Furthermore, the diameter of the analysis cell has to fit the local diameter of the vessel. Otherwise, when the cell is too small, its gravity center is not meaningful. Conversely, when the cell is too large it may contain fragments of neighboring structures that would modify the location of the gravity center. In pathologic regions, as well as near the branching points, abrupt changes of the local vessel diameter may be observed. Therefore, the diameter calculated at the previous centerline point is sometimes not suitable at the current point.

To solve this problem eigenvalues of the inertia matrix, calculated within the current cell, are analyzed to make evolve the cell size. When the cell is included within a vessel, its content has no privileged orientation and the inertia moments are identical for any axis. Conversely, when the cell is large enough to contain a cylindrical portion of the vessel, there is only one axis, corresponding to the local orientation of the vessel, around which the cylinder would spin with minimum inertia moment. Finding the appropriate size of the cell is based on the detection of the limit between the spherical and cylindrical behavior of the structure contained within the cell. The adaptation of the size of the cell is carried out by ”inflating” the cell as long as all three eigenvalues of the inertia matrix are approximately equal each to other (the cell grows within the vessel and its inertial behavior is spherical, as it contains a uniform region), or by ”deflating” it when the eigenvalues are significantly different (the cell is larger than the vessel and contains an anisotropic structure). The repositioning and resizing of the analysis cell are interleaved. After stabilization, the radius of the cell, denoted by ρ_{opt}, is approximately equal to the radius of the vessel.

Estimation of the local orientation

The local orientation of the vessel is defined by the eigenvector $\mathbf{e}_i$ associated to the smallest eigenvalue of the matrix of inertia of a cell centered in $\mathbf{x}_i$ (the current point of the axis). The radius ρ_{pred} of the sphere used for this purpose is to be large enough to encompass a portion of the vessel of interest, and small enough so that this portion be considered as approximately straight cylinder. The best experimental results are obtained when the diameter of the cell is between 1.5 and twice the vessel diameter. We fixed $\rho_{pred} = 1.5\rho_{opt}$.

Prediction

The prediction is carried out along the eigenvector $\mathbf{e}_i$ (i.e. according to the local orientation of the vessel), with amplitude δ. Our experience shows that the parameter δ is to be set approximately equal to half the local radius of the vessel: $\delta = \rho_{opt}/2$.

Stopping criteria

Two criteria are defined to properly stop the tracking of an artery when reaching its aortic origin on one side or its distal end on the other side.

When ”inflating” the analysis cell corresponding to the current end-point of the centreline (see section 2.2), the maximum value of its radius is fixed as $\rho_{max} = 15$ voxels. Beyond this value, the cell is very likely to be included within the aorta. In order to confirm it, we check whether almost all the voxels within the sphere still have typical ”arterial” intensities, i.e. more than 90% of them belong to $\mathcal{V}_{pre}$.

Similarly, when ”deflating” the cell, the minimum radius is fixed as $\rho_{min} = 2$ voxels. If less than 30% of the voxels within this sphere belong to $\mathcal{V}_{pre}$ we consider that the distal end of the artery was reached.

3 Results

The results hereafter described were obtained with a fixed set of parameters, on 24 datasets of variable quality provided by the organizers of the contest: 8 of them were available at the training stage together with reference segmentations, while the remaining 16 were only used at the testing stage. In each dataset the centerlines were extracted in four arteries: RCA, LAD, LCX and one large side branch. These centerlines

Table 1: Average overlap per training dataset

Dataset nr.	OV %	OV score	OV rank	OF %	OF score	OF rank	OT %	OT score	OT rank	Avg. rank
0	57.3	29.5	–	8.7	6.8	–	59.4	29.7	–	–
1	91.7	46.3	–	68.6	49.0	–	94.2	59.6	–	–
2	75.3	39.0	–	0.0	0.0	–	76.2	38.1	–	–
3	72.7	45.8	–	42.2	35.5	–	73.3	49.4	–	–
4	81.1	46.5	–	53.2	29.6	–	85.0	42.5	–	–
5	86.5	44.1	–	81.1	57.4	–	87.7	56.4	–	–
6	88.6	47.9	–	80.4	47.0	–	89.5	57.4	–	–
7	87.6	44.8	–	56.6	37.2	–	88.8	44.5	–	–
Avg.	**80.1**	**43.0**	**–**	**48.9**	**32.8**	**–**	**81.7**	**47.2**	**–**	**–**

Table 2: Average accuracy per training dataset

Dataset nr.	AD mm	AD score	AD rank	AI mm	AI score	AI rank	AT mm	AT score	AT rank	Avg. rank
0	10.30	20.1	–	0.45	33.2	–	10.37	20.5	–	–
1	1.51	32.2	–	0.35	34.7	–	1.08	32.8	–	–
2	4.22	21.5	–	0.34	28.8	–	4.16	21.7	–	–
3	7.99	24.9	–	0.48	33.2	–	7.78	25.0	–	–
4	4.04	22.2	–	0.36	27.0	–	3.34	23.2	–	–
5	2.07	29.7	–	0.44	34.0	–	2.04	29.9	–	–
6	2.05	24.5	–	0.32	27.8	–	2.00	24.7	–	–
7	2.39	24.7	–	0.38	27.9	–	2.24	25.0	–	–
Avg.	**4.32**	**25.0**	**–**	**0.39**	**30.8**	**–**	**4.13**	**25.3**	**–**	**–**

were then compared to reference segmentations, according to the rules of the contest specified in the CAT08 web page. The reference segmentations were calculated based on centerlines and local radii manually delineated by three experts. The tracking capability of the method was assessed by three overlap measures (tables 1 and 4): OV = overall, OF = until first failure, OT = in clinically relevant segments (radius $>$ 1.5 mm), where the semi-automatic centerline was considered as overlapping wherever its distance to the reference centerline was less than the local radius. The accuracy was also assessed by three measures (tables 2 and 5) based on the average distances between the centerlines: AD = on whole length, AI = inside the vessel (i.e. where the distance between the centerlines is less than the vessel radius), AT = in clinically relevant segments.

4 Discussion

It may be a good idea to put somewhere the URL of the Maracas page:
http://agamenon.uniandes.edu.co/~marc-her/maracas/index.html

Table 3: Summary of the results on the training datasets

Measure	% / mm min.	% / mm max.	% / mm avg.	score min.	score max.	score avg.	rank min.	rank max.	rank avg.
OV	36.5%	99.4%	80.1%	19.8	78.2	43.0	–	–	–
OF	0.0%	100.0%	48.9%	0.0	100.0	32.8	–	–	–
OT	36.5%	100.0%	81.7%	18.7	100.0	47.2	–	–	–
AD	0.30 mm	19.54 mm	4.32 mm	12.6	39.2	25.0	–	–	–
AI	0.24 mm	0.67 mm	0.39 mm	23.4	42.6	30.8	–	–	–
AT	0.29 mm	19.54 mm	4.13 mm	12.8	39.2	25.3	–	–	–
Total							**–**	**–**	**–**

Table 4: Average overlap per testing dataset

Dataset	OV			OF			OT			Avg.
nr.	%	score	rank	%	score	rank	%	score	rank	rank
8	70.8	38.6	–	38.4	28.8	–	72.6	36.4	–	–
9	88.6	45.9	–	64.3	40.2	–	89.7	57.3	–	–
10	67.4	34.4	–	40.4	20.6	–	70.3	47.7	–	–
11	91.5	59.3	–	49.5	39.4	–	91.6	59.4	–	–
12	84.0	43.4	–	7.5	3.8	–	88.6	44.6	–	–
13	81.7	41.4	–	23.4	11.7	–	83.3	54.2	–	–
14	84.7	42.9	–	22.8	14.3	–	85.2	42.6	–	–
15	90.8	46.4	–	86.3	57.0	–	93.1	59.1	–	–
16	84.8	55.2	–	54.3	40.1	–	89.3	57.2	–	–
17	64.6	37.5	–	9.5	5.3	–	66.6	34.8	–	–
18	76.4	38.7	–	69.5	56.7	–	77.4	51.3	–	–
19	79.5	41.2	–	63.1	34.5	–	79.6	39.8	–	–
20	62.9	40.6	–	14.2	7.3	–	63.4	31.8	–	–
21	91.2	46.4	–	18.1	10.0	–	95.5	48.2	–	–
22	71.8	36.2	–	60.7	30.4	–	75.2	37.6	–	–
23	91.8	46.4	–	6.8	3.4	–	91.8	45.9	–	–
Avg.	**80.2**	**43.4**	**–**	**39.3**	**25.2**	**–**	**82.1**	**46.7**	**–**	**–**

Table 5: Average accuracy per testing dataset

Dataset	AD			AI			AT			Avg.
nr.	mm	score	rank	mm	score	rank	mm	score	rank	rank
8	5.36	25.0	–	0.49	33.3	–	5.13	25.7	–	–
9	3.04	25.6	–	0.32	28.5	–	2.96	26.0	–	–
10	9.37	19.6	–	0.41	29.5	–	9.14	20.9	–	–
11	1.82	31.4	–	0.41	34.0	–	1.82	31.4	–	–
12	1.44	23.9	–	0.39	27.9	–	0.78	25.4	–	–
13	4.14	22.9	–	0.36	27.6	–	3.46	23.4	–	–
14	1.55	30.2	–	0.41	34.5	–	1.38	30.3	–	–
15	1.23	26.8	–	0.35	29.2	–	1.00	27.3	–	–
16	1.54	23.7	–	0.35	27.3	–	0.91	24.8	–	–
17	6.98	30.3	–	0.38	41.3	–	6.92	31.5	–	–
18	9.51	21.2	–	0.36	28.5	–	9.42	21.4	–	–
19	5.39	26.3	–	0.45	32.8	–	5.36	26.3	–	–
20	13.54	17.4	–	0.62	25.6	–	13.47	17.4	–	–
21	1.03	20.8	–	0.39	22.4	–	0.58	21.6	–	–
22	14.03	19.5	–	0.50	25.7	–	10.04	20.3	–	–
23	0.88	26.7	–	0.38	28.8	–	0.88	26.7	–	–
Avg.	**5.05**	**24.5**	**–**	**0.41**	**29.8**	**–**	**4.58**	**25.0**	**–**	**–**

Table 6: Summary of the results on the testing datasets

Measure	% / mm			score			rank		
	min.	max.	avg.	min.	max.	avg.	min.	max.	avg.
OV	20.5%	100.0%	80.2%	10.4	100.0	43.4	–	–	–
OF	0.0%	100.0%	39.3%	0.0	100.0	25.2	–	–	–
OT	27.9%	100.0%	82.1%	14.0	100.0	46.7	–	–	–
AD	0.31 mm	48.93 mm	5.05 mm	4.9	47.7	24.5	–	–	–
AI	0.24 mm	0.89 mm	0.41 mm	16.5	63.8	29.8	–	–	–
AT	0.25 mm	36.18 mm	4.58 mm	7.1	51.9	25.0	–	–	–
Total							**–**	**–**	**–**

References

[1] Metz C., Schaap M., van der Giessen A., van Walsum T., and Niessen W. Semi-automatic coronary artery centerline extraction in computed tomography angiography data. In *4th IEEE Int Symp Biomed Imaging*, pages 856–859, Washington DC, April 2007. 1, 2.1

[2] Lesage D., Angelini E.D., Bloch I., and Funka-Lea G. Medial-based bayesian tracking for vascular segmentation: Applicationto coronary arteries in 3D CT angigraphy. In *2008 IEEE Int Symp Biomed Imaging*, pages 268–271, Paris, France, May 2008. 1

[3] Renard F. and Yang Y. Image analysis for detection of coronary artery soft plaques in MDCT images. In *2008 IEEE Int Symp Biomed Imaging*, pages 25–28, Paris, France, May 2008. 1

[4] Li H. and Yezzi A. Vessels as 4D curves: Global minimal 4D paths to extract tubular surfaces. In *Computer Vision and Pattern Recognition Workshop*, 2006. 1

[5] Carrillo J.F., Hernández Hoyos M., Dávila E.E., and Orkisz M. Recursive tracking of vascular tree axes in 3D medical images. *Int J Comp Assisted Radiol Surg*, 1(6):331–339, 2007. 1

[6] Hernández Hoyos M., Orkisz M., Douek P.C., and Magnin I.E. Assessment of carotid artery stenoses in 3D contrast-enhanced magnetic resonance angiography, based on improved generation of the centerline. *Mach Graphics Vision*, 14(4):349–378, 2005. 1, 2.2

[7] Hernández Hoyos M., Orłowski P., Piątkowska-Janko E., Bogorodzki P., and Orkisz M. Vascular centerline extraction in 3D MR angiograms for phase contrast MRI blood flow measurement. *Int J Comp Assisted Radiol Surg*, 1(1):51–61, 2005. 2.2

[8] Aylward S.R. and Bullitt E. Initialization, noise, singularities, and scale in height ridge traversal for tubular object centerline extraction. *IEEE Trans Med Imaging*, 21(2):61–75, 2002. 1

[9] Stefan Wesarg and Evelyn A. Firle. Segmentation of vessels: The corkscrew algorithm. In J.E. Robert L. Galloway, editor, *Proceedings of SPIE International Symposium on Medical Imaging*, volume 5370, San Diego, California, February 2004. 1

Coronary centerline tracking in CT images with use of image moments and of an elastic model

Release 0.06

Marcela Hernández Hoyos[1], Maria A. Zuluaga[1,2], Mónica Lozano[1], Juan C. Prieto[1], Philippe C. Douek[2], Isabelle E. Magnin[2] and Maciej Orkisz[2]

July 7, 2008

[1]Grupo Imagine, Grupo de Ingeniería Biomédica, Universidad de los Andes, Bogota, Colombia
marc-her@uniandes.edu.co
[2]Université de Lyon; Université Lyon 1; INSA-Lyon; CNRS UMR 5220, CREATIS; Inserm U630; F-69621 Villeurbanne, France
maciej.orkisz@creatis.insa-lyon.fr

Abstract

This coronary-artery extraction method uses one initialization point per vessel. First, a mask is computed by use of a region-growing algorithm, which starts from the initial point and stops when no more connected voxels fall within an interactively defined intensity range. The centerline tracking is then performed within the mask, starting from the same initial point. This algorithm is based on a prediction/estimation scheme. It uses the first- and second-order image moments calculated within a spherical volume that slides along the vessel, and the radius of which is automatically adjusted to the local radius of the vessel. The evolution of the radius of the sphere is based on the analysis of the eigenvalues of the inertia matrix in a multi-scale framework. The estimation of the current point location makes use of an elastic model similar to "snakes". The point iteratively moves under the action of an image-force attracting it to the local gravity center, and under the reaction of the internal forces of the model, which reflect its shape constraints: continuity and smoothness. The prediction makes use of the eigenvectors of the inertia matrix. The stopping criteria of the centerline tracking are based on the size of the sphere and on the percentage of the masked voxels within the sphere.

On 8 training CT datasets, the following mean results were obtained. Overlap with reference: considering the whole length (OV) 80.1%, until the first failure (OF) 48.9%, in clinically relevant segments (radius $>$ 1.5 mm, OT) 81.7%. Average distance from reference: considering the whole length (AD) 4.32 mm, limited to segments where the semiautomatic centerline remains within the vessel (AI) 0.39 mm, in clinically relevant segments (AT) 4.13 mm. On 16 testing datasets, these results were respectively: OV $=$ 80.2%, OF $=$ 39.3%, OT $=$ 82.1%, AD $=$ 5.05 mm, AI $=$ 0.41 mm and AT $=$ 4.58 mm. A number of failures was due to the the fact that the model does not handle the bifurcations.

Latest version available at the Insight Journal [http://hdl.handle.net/1926/1401]

Contents

This paper describes a method submitted to the first Coronary Artery Tracking contest (CAT08) held in conjunction with the MICCAI 2008 conference http://miccai2008.rutgers.edu/.

Coronary artery disease remains one of the leading causes of death each year. Therefore, the evaluation of these vessels is of critical importance. Although manual delineation is still used in clinical routine, the amount of data that is processed nowadays makes automatic and semiautomatic segmentation a challenge.

Methods for centerline extraction can be broadly classified into two groups. On one hand, some methods perform an initial segmentation of the vessel followed by the centerline extraction [7]. Among these, the preferred centerline extraction technique is the skeletonization of the segmented structure. On the other hand, there are methods that perform a tracking of the centerline prior to the segmentation [8, 9] or simultaneously [1, 2, 3, 5, 6]. Main techniques used under this category include multi-scale Hessian analysis, inertia moments analysis, Bayesian approaches and minimal paths.

Some of these methods have not been originally developed to work over coronary arteries in CT images, but most of them have already been tested in this context. The main challenges still remain the correct managing of bifurcations, of severe stenoses and of adjacent hyper-intense structures.

1 Method

The core of the method is a minimally interactive centerline-tracking algorithm (section 1.2). According to the definition given by the organizers of CAT08 http://cat08.bigr.nl/, a minimally interactive algorithm is ”allowed to use one point per vessel as input”. However, our algorithm was initially developed to be used in contrast-enhanced magnetic resonance images of carotid and peripheral arteries, and is based on the assumption that the vessels are high-intensity thread-like objects on low-intensity background. As this assumption is not met in CT images representing the coronary arteries, an interactive preprocessing step was added (section 1.1), which intends to remove as much background and surrounding structures as possible. The method was implemented in a software called Maracas (Magnetic Resonance Angiography Computer Assisted Analysis http://www.creatis.insa-lyon.fr/maracas/).

1.1 Image preprocessing

The preprocessing step is actually a very coarse presegmentation that provides a connected set $\mathcal{V}_{pre}$ of voxels, the intensities of which fall within a range of values likely to correspond to arteries. A region-growing process is carried out starting from a user-defined seed point. Neighboring voxels are iteratively added to $\mathcal{V}_{pre}$ as long as they fall within a range $[T_L, T_H]$. The software starts with a preset range as proposed in [7], i.e. $T_H = 876$ HU and $T_L = 181$ HU. However, these bounds often need to be interactively adjusted, in order to cope with the variability of the intensities of lumen and calcified plaque. Starting from the preset value ($T_L = 181$ HU) the user can decrease the lower threshold, while visualizing the presegmentation result in real time, in order to check whether the subset $\mathcal{V}_{pre}$ contains the distal part of the vessel to be extracted, and to avoid the inclusion of too many neighboring structures. Similarly, the user can increase the upper threshold, in order to include the calcified plaques in the case of severe presence of calcium, and thus to avoid the apparition of "holes" in the vessel that might stop the subsequent tracking process.

1.2 Centerline-tracking algorithm

Hereafter, we give an overview of the algorithm. More details can be found in our previous publications [3, 4]. The algorithm extracts the centerline of one vessel of interest, starting from a point within its lumen, the same one that was previously used to initialize the preprocessing. It includes the following steps:

- refinement (estimation) of the current point location $\mathbf{x}_i$;
- estimation of the local orientation of the vessel $\mathbf{e}_i$;
- prediction of the next (candidate) point $\hat{\mathbf{x}}_{i+1}$ according to this orientation.

Each of them uses first- or second-order image moments computed within a spherical sub-volume called *analysis cell*. We use a multi-scale framework to determine the locally most suitable size of the cell. The iterative tracking process is carried out in two opposite directions from the starting point, and stops when one of the stopping criteria is encountered. In CT images of the coronary arteries, the tracking process is carried out within the subvolume masked by $\mathcal{V}_{pre}$, and the stopping criteria (see section *Stopping criteria*) are related to the presegmentation step.

Estimation of the current point location

Each centerline point is expected to coincide with the gravity center of the analysis cell. However, to cope with various undesired effects (noise, pathologies, nearby structures etc., we enforce continuity and smoothness of the centerline by means of a model similar to the well-known "snakes". The location of the current (predicted) point is iteratively refined under the action of an image-based *external* force and the reaction of the *internal* forces of the model. The *external* force attracts the point toward the center of gravity $\mathbf{x}_i^G$ of the cell centered in $\hat{\mathbf{x}}_i$. The *internal* forces reflect shape constraints of the model, namely continuity and smoothness, respectively weighted by coefficients w_c and w_s. The actual values of the parameters will be specified section 1.3. Hence, at j-th iteration, the corrected location of the current point is:

$$\mathbf{x}_i^j = \mathbf{x}_i^{j-1} - \left(\mathbf{x}_i^{j-1} - \mathbf{x}_i^{G,j}\right) - w_c\left(\mathbf{x}_i^{j-1} - \mathbf{x}_{i-1}\right) - w_s\left(\mathbf{x}_i^{j-1} - 2\mathbf{x}_{i-1} + \mathbf{x}_{i-2}\right), \quad (1)$$

with $\mathbf{x}_i^0 = \hat{\mathbf{x}}_i$.The displacements due to internal and external forces are iteratively recalculated as long as the resulting displacement is larger than a fixed minimum value. Furthermore, the diameter of the analysis

cell has to fit the local diameter of the vessel. Otherwise, when the cell is too small, its gravity center is not meaningful. Conversely, when the cell is too large it may contain fragments of neighboring structures that would modify the location of the gravity center. In pathologic regions, as well as near the branching points, abrupt changes of the local vessel diameter may be observed. Therefore, the diameter calculated at the previous centerline point is sometimes not suitable at the current point.

To solve this problem eigenvalues of the inertia matrix, calculated within the current cell, are analyzed to make evolve the cell size. When the cell is included within a vessel, its content has no privileged orientation and the inertia moments are identical for any axis. Conversely, when the cell is large enough to contain a cylindrical portion of the vessel, there is only one axis, corresponding to the local orientation of the vessel, around which the cylinder would spin with minimum inertia moment. Finding the appropriate size of the cell is based on the detection of the limit between the spherical and cylindrical behavior of the structure contained within the cell. The adaptation of the size of the cell is carried out by ”inflating” the cell as long as all three eigenvalues of the inertia matrix are approximately equal each to other (the cell grows within the vessel and its inertial behavior is spherical, as it contains a uniform region), or by ”deflating” it when the eigenvalues are significantly different (the cell is larger than the vessel and contains an anisotropic structure). The repositioning and resizing of the analysis cell are interleaved. After stabilization, the radius of the cell, denoted by ρ_{opt}, is approximately equal to the radius of the vessel.

Estimation of the local orientation

The local orientation of the vessel is defined by the eigenvector $\mathbf{e}_i$ associated to the smallest eigenvalue of the matrix of inertia of a cell centered in $\mathbf{x}_i$ (the current point of the axis). The radius ρ_{pred} of the sphere used for this purpose is to be large enough to encompass a portion of the vessel of interest, and small enough so that this portion be considered as approximately straight cylinder. The best experimental results are obtained when the diameter of the cell is between 1.5 and twice the vessel diameter.

Prediction

The prediction is carried out along the eigenvector $\mathbf{e}_i$, i.e. according to the orientation of the vessel, with amplitude δ (which according to our experience is to be set approximately equal to half the vessel radius):

$$\hat{\mathbf{x}}_{i+1} = \mathbf{x}_i + \delta \mathbf{e}_i. \tag{2}$$

Stopping criteria

Two criteria are defined to properly stop the tracking of an artery when reaching its aortic origin on one side or its distal end on the other side.

On the one hand, we analyze a sphere with a radius as large as $\rho_{max} = 15$ voxels, positioned at the current end-point of the centerline. This sphere is very likely to be included within the aorta if almost all the voxels within it have typical ”arterial” intensities. If more than 90% of them belong to $\mathcal{V}_{pre}$, we consider that the aortic end of the coronary artery was reached.

On the other hand, if less than 30% of the voxels within the current analysis cell (i.e. with a radius adapted to the local size of the vessel and centered at the current end-point of the centreline) belong to $\mathcal{V}_{pre}$, we consider that the distal end of the artery was reached.

Table 1: Average overlap per testing dataset

Dataset	OV			OF			OT			Avg.
nr.	%	score	rank	%	score	rank	%	score	rank	rank
8	70.8	38.6	–	38.4	28.8	–	72.6	36.4	–	–
9	88.6	45.9	–	64.3	40.2	–	89.7	57.3	–	–
10	67.4	34.4	–	40.4	20.6	–	70.3	47.7	–	–
11	91.5	59.3	–	49.5	39.4	–	91.6	59.4	–	–
12	84.0	43.4	–	7.5	3.8	–	88.6	44.6	–	–
13	81.7	41.4	–	23.4	11.7	–	83.3	54.2	–	–
14	84.7	42.9	–	22.8	14.3	–	85.2	42.6	–	–
15	90.8	46.4	–	86.3	57.0	–	93.1	59.1	–	–
16	84.8	55.2	–	54.3	40.1	–	89.3	57.2	–	–
17	64.6	37.5	–	9.5	5.3	–	66.6	34.8	–	–
18	76.4	38.7	–	69.5	56.7	–	77.4	51.3	–	–
19	79.5	41.2	–	63.1	34.5	–	79.6	39.8	–	–
20	62.9	40.6	–	14.2	7.3	–	63.4	31.8	–	–
21	91.2	46.4	–	18.1	10.0	–	95.5	48.2	–	–
22	71.8	36.2	–	60.7	30.4	–	75.2	37.6	–	–
23	91.8	46.4	–	6.8	3.4	–	91.8	45.9	–	–
Avg.	**80.2**	**43.4**	**–**	**39.3**	**25.2**	**–**	**82.1**	**46.7**	**–**	**–**

Table 2: Average accuracy per testing dataset

Dataset	AD			AI			AT			Avg.
nr.	mm	score	rank	mm	score	rank	mm	score	rank	rank
8	5.36	25.0	–	0.49	33.3	–	5.13	25.7	–	–
9	3.04	25.6	–	0.32	28.5	–	2.96	26.0	–	–
10	9.37	19.6	–	0.41	29.5	–	9.14	20.9	–	–
11	1.82	31.4	–	0.41	34.0	–	1.82	31.4	–	–
12	1.44	23.9	–	0.39	27.9	–	0.78	25.4	–	–
13	4.14	22.9	–	0.36	27.6	–	3.46	23.4	–	–
14	1.55	30.2	–	0.41	34.5	–	1.38	30.3	–	–
15	1.23	26.8	–	0.35	29.2	–	1.00	27.3	–	–
16	1.54	23.7	–	0.35	27.3	–	0.91	24.8	–	–
17	6.98	30.3	–	0.38	41.3	–	6.92	31.5	–	–
18	9.51	21.2	–	0.36	28.5	–	9.42	21.4	–	–
19	5.39	26.3	–	0.45	32.8	–	5.36	26.3	–	–
20	13.54	17.4	–	0.62	25.6	–	13.47	17.4	–	–
21	1.03	20.8	–	0.39	22.4	–	0.58	21.6	–	–
22	14.03	19.5	–	0.50	25.7	–	10.04	20.3	–	–
23	0.88	26.7	–	0.38	28.8	–	0.88	26.7	–	–
Avg.	**5.05**	**24.5**	**–**	**0.41**	**29.8**	**–**	**4.58**	**25.0**	**–**	**–**

1.3 Parameter settings

The best empiric values of the parameters of the model were fixed as follows: $w_c = 0.5$ (rather low elasticity), $w_s = 0.1$ (rather high flexibility). The estimation of the orientation and the prediction used the aforementioned ratios: $\rho_{pred} = 1.5\rho_{opt}$, $\delta = \rho_{opt}/2$. As for the intensity thresholds used at the preprocessing step, the interactively adjusted values were on average as follows: $T_L = 150 \pm 38$ HU, $T_H = 1020 \pm 310$ HU.

2 Results

The results hereafter described were obtained on 24 datasets of variable quality provided by the organizers of the contest: 8 of them were available at the training stage together with reference segmentations, while the remaining 16 were only used at the testing stage. In each dataset the centerlines were extracted in four arteries: RCA, LAD, LCX and one large side branch. These centerlines were then compared to reference segmen-

Table 3: Summary of the results on the testing datasets

Measure	% / mm			score			rank		
	min.	max.	avg.	min.	max.	avg.	min.	max.	avg.
OV	20.5%	100.0%	80.2%	10.4	100.0	43.4	–	–	–
OF	0.0%	100.0%	39.3%	0.0	100.0	25.2	–	–	–
OT	27.9%	100.0%	82.1%	14.0	100.0	46.7	–	–	–
AD	0.31 mm	48.93 mm	5.05 mm	4.9	47.7	24.5	–	–	–
AI	0.24 mm	0.89 mm	0.41 mm	16.5	63.8	29.8	–	–	–
AT	0.25 mm	36.18 mm	4.58 mm	7.1	51.9	25.0	–	–	–
Total							**–**	**–**	**–**

Table 4: Summary of the results on the training datasets

Measure	% / mm			score			rank		
	min.	max.	avg.	min.	max.	avg.	min.	max.	avg.
OV	36.5%	99.4%	80.1%	19.8	78.2	43.0	–	–	–
OF	0.0%	100.0%	48.9%	0.0	100.0	32.8	–	–	–
OT	36.5%	100.0%	81.7%	18.7	100.0	47.2	–	–	–
AD	0.30 mm	19.54 mm	4.32 mm	12.6	39.2	25.0	–	–	–
AI	0.24 mm	0.67 mm	0.39 mm	23.4	42.6	30.8	–	–	–
AT	0.29 mm	19.54 mm	4.13 mm	12.8	39.2	25.3	–	–	–
Total							**–**	**–**	**–**

tations, according to the rules of the contest specified in the CAT08 web page http://cat08.bigr.nl/. The reference segmentations were calculated based on centerlines and local radii manually delineated by three experts. The tracking capability of the method was assessed by three overlap measures (table 1): OV = overall, OF = until first failure, OT = in clinically relevant segments (radius > 1.5 mm), where the semi-automatic centerline was considered as overlapping wherever its distance to the reference centerline was less than the local radius. The accuracy was also assessed by three measures (table 2) based on the average distances between the centerlines: AD = on whole length, AI = inside the vessel (i.e. where the distance between the centerlines is less than the vessel radius), AT = in clinically relevant segments. The results obtained on the training and testing datasets were very similar and are respectively summarized in tables 4 and 3. Figure 1 shows an example of the centerlines extracted by our method (blue) superimposed onto the reference centerlines (white = RCA, yellow = LAD, green = LCX, red = diagonal branch of LAD). The corresponding average overlap and distance measures were as follows:
– dataset 4: OV = 81.1%, OF = 53.2%, OT = 85.0%, AD = 4.04 mm, AI = 0.36 mm, AT = 3.34 mm;
– dataset 6: OV = 88.6%, OF = 80.4%, OT = 89.5%, AD = 2.05 mm, AI = 0.32 mm, AT = 2.00 mm.

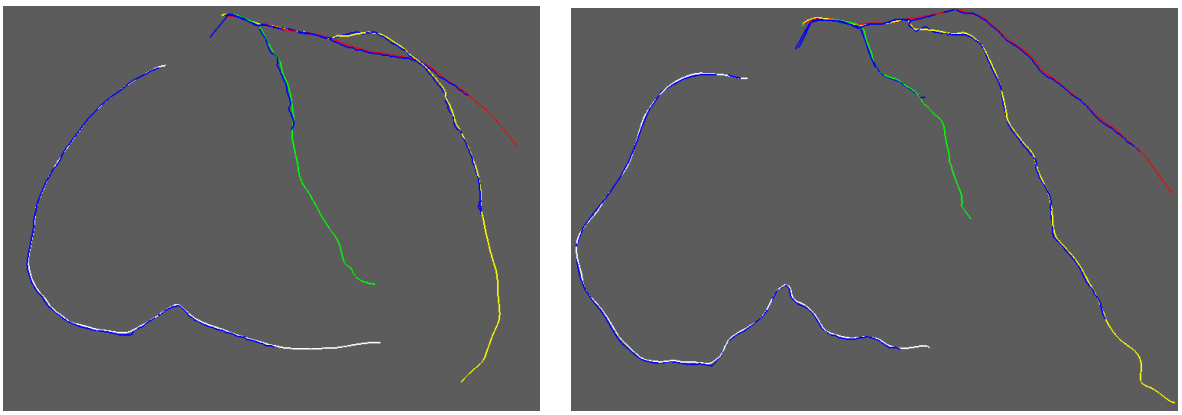

Figure 1: Examples of centerlines obtained with our method (blue) superimposed onto the reference centerlines (white = RCA, yellow = LAD, green = LCX, red = diagonal branch of LAD): datasets 4 (left) and 6 (right).

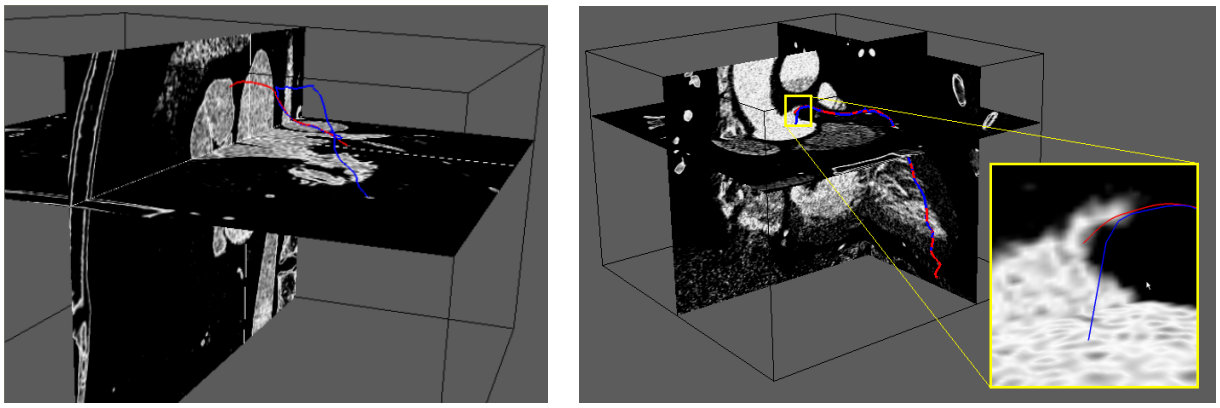

Figure 2: Examples of failures. Left (dataset 06, LCX): the semiautomatic centerline (blue) correctly follows the reference one (red) in the LCX until it reaches the common trunk of the LCA, then it turns toward the distal part (LAD), thus failing to reach the aorta. Right (dataset 1, LAD): while the overall overlap between blue and red centerlines is good OV $= 91.4\%$, the semi-automatic centerline makes a "shortcut" toward the high-intensity interior of the aorta, which results in OF $= 0.0\%$.

3 Discussion and conclusion

One of the principal difficulties in this type of images is the detection of the distal end of the artery, where the limitations of image contrast and resolution are reached. The point annotated as artery end usually corresponds to the absence of signal rather than to the anatomic very end of the vessel. However, signal gaps may occur earlier on the arterial pathway, owing to stenoses, artifacts or noise. When our algorithm encounters a gap it stops, while a human expert is able to use his(her) anatomic knowledge in order to scan an appropriate region seeking a possible continuation of the artery. Hence, one possible perspective to improve our method is to include some anatomic prior and to mimic the expert's reasoning.

Despite this limitation, the overall tracking capability (OV) of our algorithm is quite correct. However, the scores OF were rather low, owing to several vessels with OF $= 0.0\%$, which means that the very first point of such centerlines is not correctly located on the boundary of the aorta. This occurs in two situations.

The first one (fig. 2 left) can be explained by the fact that our model does not manage bifurcations. When a centerline initialized in a secondary branch (e.g. LCX or diagonal branch of LAD) reaches the primary branch, it may turn toward its distal (instead of proximal) part, and thus never reach the aorta. Once again, the addition of some anatomic prior might avoid this kind of errors.

In the second situation (fig. 2 right) the very last point of the centerline is strongly attracted by the aorta, since the gravity center falls within this large hyperintense structure. The analysis cell grows trying to adapt itself to the sudden change of vessel size. Consequently, the gravity center iteratively moves further into the aorta toward its most intense part, which is not necessarily in front of the coronary artery. We will intend to solve this problem by adaptively increasing the coefficients w_c and w_s of the model whenever a sudden increase of the analysis-cell radius will be detected. Let us note that in both situations the centerline might be easily corrected by interactively placing and additional point. However, we refrained ourselves from other interaction than the initial adjustment of the thresholds and the definition of one starting point per artery.

As for the accuracy, the average scores were rather low. We identified two sources of large errors: 1) in bifurcations the algorithm sometimes "hesitates" between the two branches, 2) in calcified regions the centerline is attracted by the hyperintense plaque. While the first of these problems is likely to be solved by

a relatively simple postprocessing of the centerline, the latter requires a more careful design. Beyond the bifurcations and calcified regions, we frequently observed that the semi-automatic centerline was parallel to the reference one at approximately one-voxel distance. This may be a numerical implementation problem.

In conclusion, our method requires a small quantity of interaction: initial adjustment of two thresholds (if necessary) and placing of one starting point per artery. Its tracking capability is satisfactory and still can be improved, either by the aforementioned modifications of the algorithm, or by additional interaction. The accuracy is less satisfactory and requires a careful revision of the model and of the implementation.

References

[1] S.R. Aylward and E. Bullitt. Initialization, noise, singularities, and scale in height ridge traversal for tubular object centerline extraction. *IEEE Trans Med Imaging*, 21(2):61–75, 2002. (document)

[2] J.F. Carrillo, M. Hernández Hoyos, E.E. Dávila, and M. Orkisz. Recursive tracking of vascular tree axes in 3D medical images. *Int J Comp Assisted Radiol Surg*, 1(6):331–339, 2007. (document)

[3] M. Hernández Hoyos, M. Orkisz, P.C. Douek, and I.E. Magnin. Assessment of carotid artery stenoses in 3D contrast-enhanced magnetic resonance angiography, based on improved generation of the centerline. *Mach Graphics Vision*, 14(4):349–378, 2005. (document), 1.2

[4] M. Hernández Hoyos, P. Orłowski, E. Piątkowska-Janko, P. Bogorodzki, and M. Orkisz. Vascular centerline extraction in 3D MR angiograms for phase contrast MRI blood flow measurement. *Int J Comp Assisted Radiol Surg*, 1(1):51–61, 2005. 1.2

[5] D. Lesage, E.D. Angelini, I. Bloch, and G. Funka-Lea. Medial-based bayesian tracking for vascular segmentation: Application to coronary arteries in 3D CT angiography. In *2008 IEEE Int Symp Biomed Imaging*, pages 268–271, Paris, France, May 2008. (document)

[6] H. Li and A. Yezzi. Vessels as 4D curves: Global minimal 4D paths to extract tubular surfaces. In *Computer Vision and Pattern Recognition Workshop*, 2006. (document)

[7] C. Metz, M. Schaap, A. van der Giessen, T. van Walsum, and W. Niessen. Semi-automatic coronary artery centerline extraction in computed tomography angiography data. In *4th IEEE Int Symp Biomed Imaging*, pages 856–859, Washington DC, April 2007. (document), 1.1

[8] F. Renard and Y. Yang. Image analysis for detection of coronary artery soft plaques in MDCT images. In *2008 IEEE Int Symp Biomed Imaging*, pages 25–28, Paris, France, May 2008. (document)

[9] S. Wesarg and E.A. Firle. Segmentation of vessels: The corkscrew algorithm. In J.E. Robert L. Galloway, editor, *Proceedings of SPIE International Symposium on Medical Imaging*, volume 5370, San Diego, California, February 2004. (document)